Optical Properties of Chiral Three-Dimensional Plasmonic Oligomers at the Onset of Charge-Transfer Plasmons

Mario Hentschel,[†,‡,*] Lin Wu,[§] Martin Schäferling,[†] Ping Bai,[§] Er Ping Li,[§] and Harald Giessen[†]

[†]4th Physics Institute and Research Center SCoPE, University of Stuttgart, Pfaffenwaldring 57, 70569 Stuttgart, Germany, [‡]Max Planck Institute for Solid State Research, Heisenbergstrasse 1, 70569 Stuttgart, Germany, and [§]Institute of High Performance Computing, A*STAR (Agency for Science, Technology and Research), 1 Fusionopolis Way, #16-16 Connexis North, Singapore 138632

ABSTRACT We demonstrate strong chiral optical response in three-dimensional chiral nanoparticle oligomers in the wavelength regime between 700 and 3500 nm. We show in experiment and simulation that this broad-band response occurs at the onset of charge transfer between the individual nanoparticles. The ohmic contact causes a strong red shift of the fundamental mode, while the geometrical shape of the resulting fused particles still allows for an efficient excitation of higher order modes. Calculated spectra and field distributions confirm our interpretation and show a number of interacting plasmonic modes. Our results deepen the understanding of the chiral optical response in complex chiral plasmonic nanostructures and pave the road toward broad-band chiral optical devices with strong responses, for example, for chiral plasmon rulers or sensing applications.

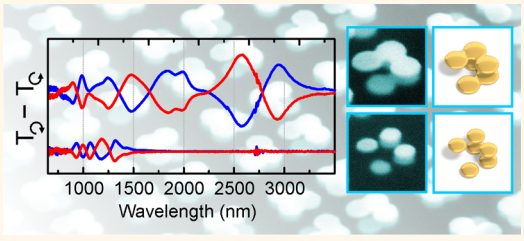

KEYWORDS: plasmons · circular dichroism · oligomers · chirality stereochemistry · enantiomers · charge-transfer plasmon

Chirality has gathered significant interest in different fields of research due to its fundamental importance in nature and living matter. Chirality has two distinctive meanings. On the one hand, it refers to a simple geometrical property: a chiral object cannot be superimposed with its mirror image. The original structure and the mirror image are called the two enantiomers of a chiral compound. For example, many biomolecules are handed, and some occur only in one of the possible handed forms. On the other hand, chirality can manifest itself optically, namely, in a different response of a chiral structure to left- or right-handed circularly polarized light. The interaction of chiral molecules or structures with circularly polarized light in turn causes a multitude of intriguing phenomena, such as circular dichroism (CD) or optical rotatory dispersion (ORD).[1]

Most naturally occurring chiral optical phenomena are intrinsically weak. Chiral molecules have small dipole moments and hence couple only weakly to an external light field. Sugar solution, for example, is known to cause comparably strong optical polarization rotation; nevertheless, centimeters of solution at molar concentrations are needed for efficient rotation of linear polarization. Similarly, it is challenging to study chiral molecules or even to optically discriminate enantiomers.

Recently, it has been proposed that plasmonics (*i.e.*, the optics of metal nanoparticles) might help in overcoming some of these fundamental limitations. Such nanoparticles are known for their highly efficient interaction with an external light field. This property is caused by the large dipole moments of the plasmonic resonances which fundamentally stem from the collective oscillation of the quasi-free conduction electrons. In particular, the interaction strength with an external light field surpasses the one for molecules by orders of magnitude. Accordingly, it has been recently demonstrated that the chiral optical response of three-dimensional plasmonic nanostructures is significantly enhanced.[2−15] Moreover, it has been demonstrated that even handed planar plasmonic structures show huge chiral interaction with circularly polarized light despite the fact that they are not truly chiral.[16−22]

* Address correspondence to m.hentschel@physik.uni-stuttgart.de.

Received for review September 17, 2012 and accepted October 18, 2012.

Published online October 18, 2012
10.1021/nn304283y

In contrast to molecules, complex plasmonic oligomers composed of noble metal nanoparticles allow for a nearly arbitrary manipulation of their constitution and configuration.[23] This amazing potential enables us to design and tailor the optical response of plasmonic structures nearly at will.[24−30] We can thus optimize the property of a given structure in order to meet the needs of the intended application, for example, for plasmonic sensing.[31−34]

Recently, it has been shown that in the vicinity of chiral plasmonic structures electromagnetic fields with strong optical chirality are formed,[35−38] which strongly interact with chiral molecules. It has been proposed that these fields might ultimately enable the detection of individual chiral molecules and their discrimination due to a significantly enhanced interaction of the molecules with the external light field mediated by the plasmonic nanostructure.[39−42] Nevertheless, these experimental studies are at the very beginning and yet need to be fully understood. An in-depth understanding of the underlying processes and an intuitive design strategy for maximum interaction and sensing sensitivity still needs to be developed. In any case, for a fundamental understanding of chirality in plasmonic systems and for applications of such chiral optical phenomena, it is highly intriguing to study the prerequisites for a maximized chiral optical response in the far-field. Apart from a maximized circular dichroism, spectral tunability or the possibility for broadband operation is attractive.

In this article, we demonstrate that the concept of chiral plasmonic oligomers[43] composed of individual metal nanoparticles arranged in a handed fashion is particularly suited to control bandwidth and chirality. Furthermore, we show that the chiral optical response of these oligomers is greatly enhanced in magnitude and spectral bandwidth once the individual particles touch each other, allowing for the excitation of a charge-transfer plasmon.[44−48] This ohmic connection on the one hand causes a significant red shift of the fundamental resonance of the structure. On the other hand, due to the irregular shape of the resulting fused particles, higher order modes can be efficiently excited.[49,50] Both cause an experimental chiral optical response of the oligomers between about 700 and 3500 nm.

RESULTS AND DISCUSSION

The most prominent example of a chiral structure is a helix (cf. Figure 1a). Yet, the fabrication of such 3D structures remains challenging. Impressive work has been done utilizing direct laser writing[51] and subsequent gold plating to obtain solid metal structures,[2,3] dielectric matrixes or polymers,[52,53] helixes formed by block copolymers,[54,55] or electroless plating of a dielectric chiral matrix.[4] However, the miniaturization of these helixes in order to obtain a chiral optical response in the near-infrared or even visible wavelength regime has not yet been demonstrated. A straightforward idea, however, is to replace the helix with individual nanoparticles arranged in a handed fashion, as sketched in Figure 1a. The depicted arrangement of six particles can be viewed as the first winding of a helix. The benefit afforded by this strategy is three-fold. First, the fabrication of such structures is possible by self-assembly techniques[56−60] as well as multilayer electron-beam lithography.[5,43,61] Second, the fundamental plasmonic modes of the structure are significantly blue-shifted due to reduced coupling. Instead of conductive coupling, as in the case of a solid helix, the particles interact *via* their respective near-fields. Third, the spectral regime in which the chiral optical response occurs can be nearly arbitrarily shifted by changing the particle size and by choice of the appropriate metal.[62−64]

A helix is better approximated if more particles and more layers are utilized. In practice, both quantities are limited by experimental feasibility. Figure 1b depicts artist's impressions as well as tilted view scanning electron microscope (SEM) images of our fabricated structures. The structures consist of two layers fabricated by electron-beam lithography (for details, please refer to the Methods section).[65] Both layers contain three particles arranged in an L-shape. The layers are twisted with respect to one another, which determines the handedness of the resulting structure. Changing the size of the individual particles allows tuning of the coupling strength within each layer. An increase in particle diameter will increase the coupling due to closing of the interparticle gap. As soon as the particles touch, the coupling mechanism within the layers changes from capacitive (*i.e.*, near-field coupling) to conductive coupling which leads to the formation of a charge-transfer mode.[66] Thus, one can laterally merge the dots of each layer, which significantly increases the coupling strength and the dipole moment of the resulting resonances. Moreover, it further improves the approximation of a helix. Figure 1c shows a tilted overview SEM image of our fabricated oligomer. The four elements of the unit cell are arranged in a C_4-symmetric fashion and thus form a uniaxial lattice which suppresses contributions of polarization conversion.[61] This prerequisite is of utmost importance for our measurements. In order to characterize chiral structures, one normally examines the circular dichroism (CD) spectra which are defined as the difference in absorbance for left- and right-handed circularly polarized light.[67] Our setup (for details, see the Methods section) is not capable of measuring the reflectance of circularly polarized light for the large required wavelength range. Therefore, we need to rely on transmittance measurements and thus define the quantity ΔT as the difference in transmittance T_{RCP} and T_{LCP} for right- and left-handed circularly polarized light. As we ensured the uniaxiality of the superstructure, we can

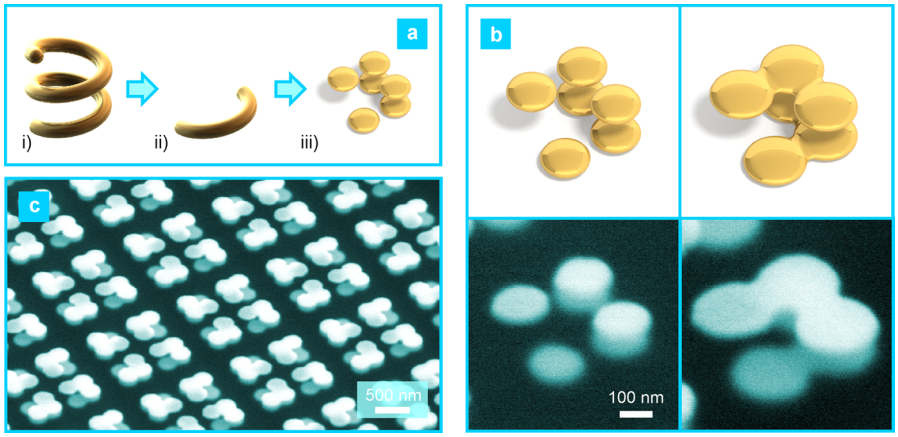

Figure 1. (a) A helix is a prototype chiral structure. In order to experimentally realize such a configurationally chiral structure, one can approximate the first winding of the helix by a handed arrangement of individual nanoparticles. (b) Our fabricated structures consist of two twisted layers, each containing three particles arranged in an L-shape (artist's impression in the top row, SEM micrographs of the fabricated structures in the bottom row). This design furthermore allows merging the particles into one another, increasing the coupling strength. (c) Tilted overview SEM image of a fabricated array. The structures are arranged in a C_4-symmetric and thus uniaxial lattice in order to suppress contributions of polarization conversion.

assume any contribution of polarization conversion to be negligible, hence the transmittance difference ΔT is directly correlated to CD.[43]

In order to study the chiral optical response of our oligomers, we have successively increased the size of the individual particles. Figure 2 depicts the transmittance spectra for right- and left-handed circularly polarized light for three different particle sizes. The lowest spectra show the response of an oligomer with well-separated particles. The response is thus described in terms of capacitive coupling, that is, near-field coupling. We observe strongly modulated spectra in the red and near-infrared part of the spectrum with a number of different modes and a pronounced difference for the two different circular polarizations. This already indicates strong chiral optical interaction. The topmost spectra illustrate the case of fully touching particles and are thus characterized by conductive coupling and the appearance of the charge-transfer plasmon. First, we notice a significant red shift of the fundamental plasmon mode from about 1200 to 3000 nm. This behavior is expected as the length of the merged particles increases upon charge transfer. However, we as well observe a number of additional resonances in the red and near-infrared wavelength range. Even in the red spectral region, these resonances show strong modulation which is comparable to the response of the oligomer with well-separated particles. Overall, the differences for the two polarizations are even stronger in the conductively coupled case. The middle spectra depict the case for just touching particles. Due to fabrication tolerances, not all particles are actually touching, which allows us to observe the transition from the capacitively coupled to the conductively coupled case. Consequently, the spectra show the formation of the new lowest energy modes, while the modes of the separated oligomer are still partially visible.

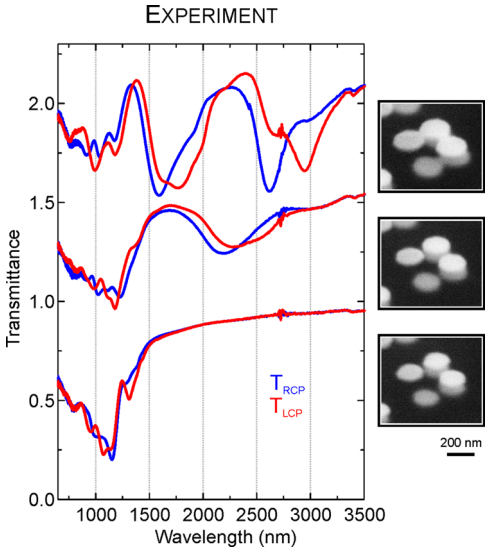

Figure 2. Transmittance spectra for right- and left-handed circularly polarized light for oligomers with different diameter of the constituting particles as well as tilted view SEM images of the corresponding structures. The bottom depicts the case of well-separated particles, the middle just touching particles, and the top the case of completely fused particles. The spectra are shifted upward in steps of 0.7 for clarity.

In order to directly compare the chiral optical response of the oligomers upon increasing particle size, we plot the experimental $\Delta T = T_{RCP} - T_{LCP}$ spectra for both enantiomers in the left column of Figure 3. Compared to Figure 2, we show additional oligomers with intermediate particles sizes which allows for a better understanding and visualization of the transition behavior. The red and blue spectra correspond to the left- and right-handed enantiomers of each oligomer. For all cases, we observe excellent mirror symmetry of the ΔT spectra, which is expected for interchanged handedness. The two lowest oligomers correspond to

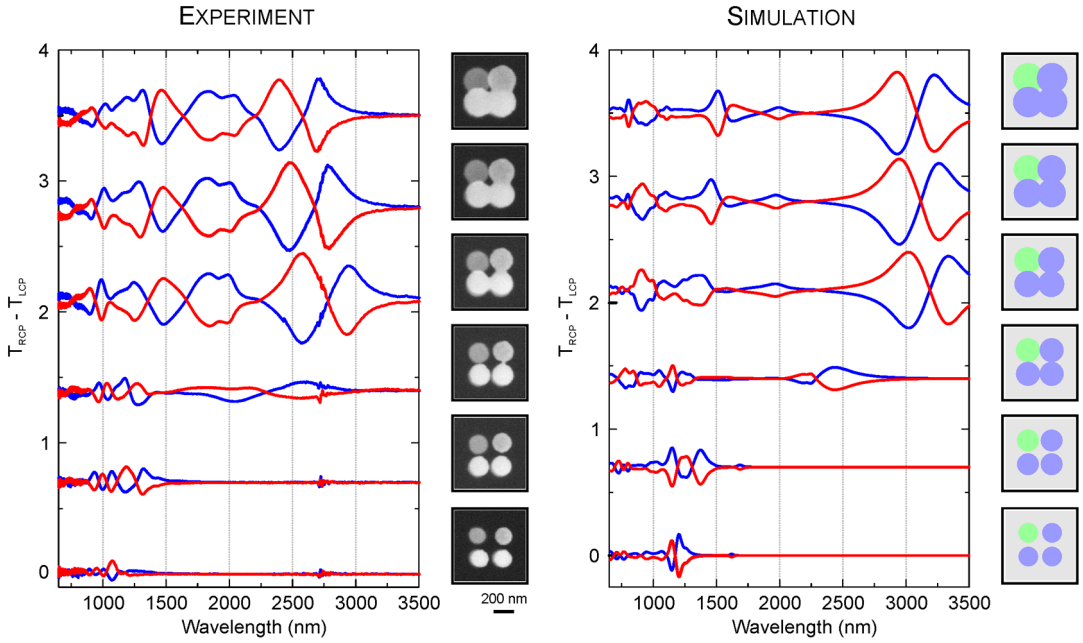

Figure 3. Experimental (left) and simulated (right) ΔT spectra, defined as the difference in the transmittance of right- and left-handed circularly polarized light. The red and blue spectra correspond to the left- and right-handed enantiomers, respectively. In experiment and simulation, one observes the appearance of a new fundamental and a number of higher order modes upon the increase of the size of the constituting particles (cf. the normal view SEM images and sketches). The reason is the transition from capacitive to conductive coupling and thus the appearance of a charge-transfer mode. The difference in the transmittance of right- and left-handed circularly polarized light reaches values as high as 35%. The spectra are shifted upward in steps of 0.7 for clarity.

the case of fully separated particles and thus to the near-field coupled regime. The coupling strength increases with increasing diameter as the spectral features are red-shifting. Yet, the overall mode structure remains unchanged. The next set of spectra shows the transition regime between capacitive and conductive coupling. Inspection of normal view SEM micrographs indicates that only about ~50% of the particles are actually touching. Despite this uncertainty, the mirror symmetry between the spectra of the two enantiomers is still excellent, indicating that the fraction of touching particles is about equal. With further increase of the size of the individual particles, they start to fully merge. We observe the formation of an extremely strong and broad-band chiral optical response between roughly 700 and 3500 nm, which corresponds to a bandwidth of more than 2 octaves. The transmittance difference reaches values up to nearly 35%. The reason for the strong chiral optical response is most likely connected to the strongly increased dipole moment of the plasmonic resonances. The L-shaped particle which forms due to the merging of the individual particles possesses a significantly larger volume and thus a larger number of quasi-free conduction electrons and consequently a larger dipole moment of its plasmonic modes. Further increasing the size of the particles leads to a spectral shift of the resonances but no longer to a significant change in the mode structure, as the overall geometrical shape of the structure no longer changes. We expect that the mode structure will only significantly change again when the dotted L-shaped particle approaches a perfect undistorted L-shape. Additionally, one observes a blue shift of the plasmonic resonances in the spectra, which is particularly obvious for the lowest energy modes. Intuitively, one would have expected a red shift due to the increased size of the merged particle. Yet, this red shift is overcompensated by the blue shift of the plasmon modes upon increase of the width of the structures, which is accompanied by the size increase of the individual particles.

All of our experimental findings are confirmed by numerical calculations, which agree very well (cf. Figure 3, right column). In brief, finite element simulation method[68] is used to solve the three-dimensional Maxwell's equations (for details, please refer to the Methods section). The transmittances to the right- or left-handed circularly polarized light are simulated for each oligomer, and the differences ΔT are obtained accordingly. The initial red shift of the resonances and the later blue shift are well reproduced. Overall, we observe a few small deviations. In particular, the simulation predicts a significantly larger spectral separation between the fundamental resonance and the higher order modes. Yet, the overall mode profiles are very well reproduced. We attribute the differences to the highly complex shape of the nanoparticles and the complex structure and arrangements. Small deviations between the simulated and measured structural geometry, which are well within the tolerances of the fabrication techniques, might cause already significant deviations.

So far, the appearance of the higher order modes remains unclear. Intuitively, one would expect an overall red shift of all modes and therefore the disappearance of a chiral optical response in the red and near-infrared. The experimental spectra in Figure 4 are capable of explaining the observed phenomenon. As a reference, we fabricated single-layered structures, which are separated particles, merged particles, and a perfect L-shape. The spectra have been obtained under excitation with linear polarized light, polarized under 45° with respect to the lattice. Note that the structures are still arranged in a C_4-symmetric lattice, despite the fact that only one structure is depicted in the corresponding SEM micrograph for clarity. For the isolated particles (black), we observe a number of resonances which are all well below 1500 nm in resonance wavelength. The perfect L-shape (blue) exhibits three pronounced resonances. These resonances correspond to the three fundamental split-ring resonator (SRR) modes as the L-shape resembles a SRR.[69] When turning to the case of the merged particle depicted in the middle row, we observe a combination of the two previously mentioned extreme cases. The L-shape is distorted by the waists of the individual merged particles. Indeed, the corresponding spectrum exhibits a number of additional higher order modes. This fact explains the presence of the higher order modes in the red and near-infrared region in the chiral optical response of the two-layered oligomers. All observed modes are caused by the hybridization of the modes of the individual building blocks. An increased number of modes supported by the building blocks will lead to a larger number of hybridized collective modes of the oligomer. *The true benefit afforded by the distorted L-shape is thus the ability to support a large number of different modes which retain significant resonance dipole moment and thus couple efficiency to an external light field.*

In order to further elucidate this experimental finding, we simulated the optical response of the individual building blocks of our chiral plasmonic oligomers. Figure 5 depicts the transmittance spectra as well as near-field intensity maps of the isolated particles and the perfect L-shape under circularly polarized excitation. The far-field optical response of the structures is identical for left- and right-handed circularly polarized incident light. This behavior is expected as the structures are achiral and the arrangement is uniaxial. Thus, one observes neither circular dichroism nor polarization conversion. Both spectra exhibit two main and well-modulated resonances. The lowest energy mode A of the isolated particle structure is a combination of dipolar excitations in the individual particles, leading to a mode that can be characterized as a bonding dipole mode. The higher energy mode B in contrast is characterized by strong quadrupolar excitations, leading to a bonding quadrupole type mode. The perfect L-shape on the other hand shows much simpler mode behavior.

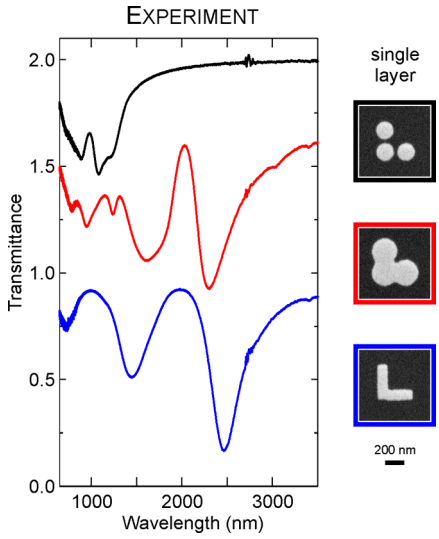

Figure 4. Transmittance spectra under linear polarized excitation for single-layered reference structures, which are isolated particles, merged particles, and a perfect L-shape. The dotted L-shape combines the benefits from the isolated dots and the perfect L-shape: a large number of resonances can be observed. The spectra are shifted upward for clarity (the spectrum of the isolated particles by 1, the merged particles by 0.8).

As expected, we observe a $\lambda/2$ (C) and a λ (D) mode as the two fundamental standing wave type modes of a wire. Higher order standing wave modes are most likely present, yet their modulation is weak. The excitation of these modes depends strongly on the resonance dipole moment associated with it, which is expected to drop significantly for increasing mode order.[69]

In order to understand the complex yet intriguing behavior of the three-dimensional oligomers, we now turn our attention to the case of the merged three-particle structure. Figure 6 depicts the simulated transmittance spectra as well as the calculated near-field intensity maps. Again, we observe an identical far-field optical response for left- and right-handed circularly polarized excitation. However, in contrast to the previous case, we observe a number of well-modulated resonances, in good agreement with our experimental results shown in Figure 4. Interestingly, the mode structure of the distorted L-shape is a combination of the modes found in the structures of Figure 5. The two lowest energy modes at spectral positions A and B are $\lambda/2$ and λ modes. In contrast to the perfect L-shape, we as well observe a well-modulated $3\lambda/2$ mode at spectral position C. The waists of the structure perfectly match the profile of this $3\lambda/2$ mode. Thus, the mode retains a significantly stronger resonance dipole moment facilitating its excitation. Additionally, we observe bonding dipole and bonding quadrupole type modes at spectral positions D and E, which are, again, enabled by the distortions induced by fusing the three individual particles into the L-shape. Thus, we can deduce from the calculations that the *distorted L-shape*

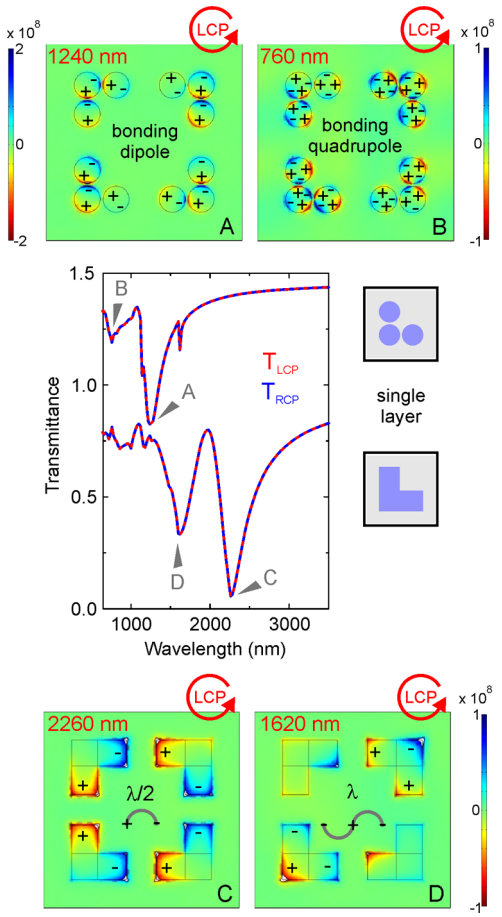

Figure 5. Simulated far- and near-field optical response of single-layer isolated particles and perfect L-shape structures under circularly polarized excitation. The transmittance spectra for left- and right-handed circularly polarized incident light are identical, as to be expected for an achiral and uniaxial structure. The near-field plots reveal bonding dipole and quadrupole type modes for the three-particle structure and standing wave type modes for the perfect L-shape. The near-field plots are depicted for left-handed circularly polarized excitation, as indicated by the red arrow. The topmost spectrum is shifted upward by 0.5 for clarity.

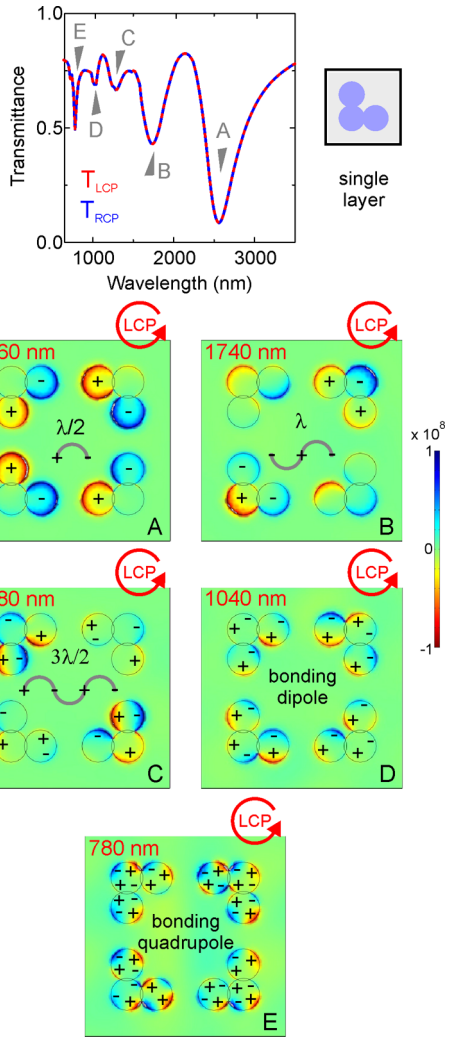

Figure 6. Simulated far- and near-field optical response of a single-layer merged L-shape structure under circularly polarized excitation. The transmittance spectra for left- and right-handed circularly polarized incident light are identical, as to be expected for an achiral and uniaxial structure. We observe a number of well-modulated resonances. The corresponding modes are a combination of the isolated three-particle and the perfect L-shape cases. We observe $\lambda/2$, λ, $3\lambda/2$ standing wave type modes and simultaneously bonding dipole and bonding quadrupole type modes.

combines the benefits from both the isolated three-particle structure and the perfect L-shape, underlining the experimental findings of Figure 4.

As we now have a clear understanding of the mode structure of the individual layers, we can attempt to unravel the mode structure of the double-layered chiral structures. First, we will examine the case of the fully fused distorted L-shape in Figure 7. The top part depicts the calculated transmittance spectra for left- and right-handed circularly polarized excitation as well as the calculated $\Delta T = T_{RCP} - T_{LCP}$ spectrum. The bottom part shows near-field distributions at four selected spectral positions. The color of the surrounding frame and arrow indicates the polarization of the excitation (blue = RCP, red = LCP). Intuitively, we expect the modes of the structure to be combinations of the modes of the individual building blocks. In order to elucidate this behavior, we first turn our attention to the fundamental mode of the structure. We clearly see that this mode strongly splits in resonance energy depending on the polarization of the incoming light. If we examine the field plots at spectral positions A and B, we see that the modes are of similar character yet show different phase behavior. Both modes are combinations of the fundamental $\lambda/2$ mode of the merged L-shape. Under right-handed circularly polarized excitation, the modes of the individual layers are in phase, whereas they are in antiphase for left-handed circularly polarized excitation. We can associate each mode with an induced ring current that is flowing along the particle shape. In order to understand the energy splitting, it is most intuitive to consider the magnetic

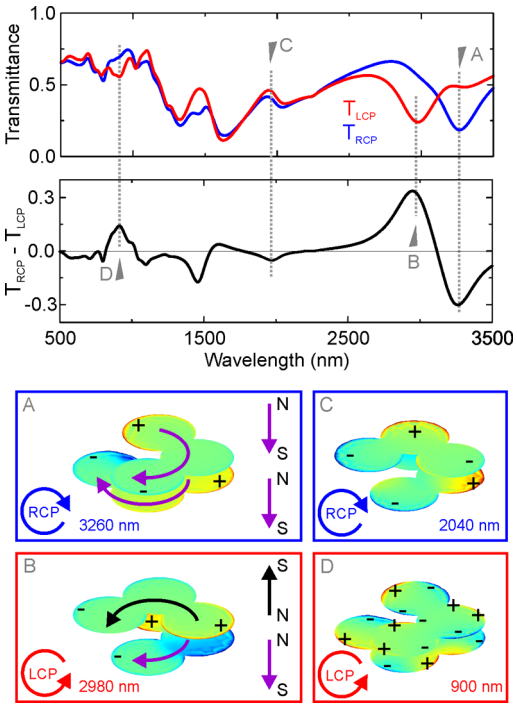

Figure 7. Calculated near- and far-field optical response of a two-layered chiral plasmonic oligomer, consisting of fused together L-shapes. The two lowest energy modes at spectral positions A and B correspond to the combination of the fundamental $\lambda/2$ modes of the individual layers. The lowest energy mode is characterized by a parallel arrangement of the magnetic moments induced by the ring currents in the particles, and the higher energy mode shows an antiparallel arrangement. The modes at spectral positions C and D are the combination of the λ modes and the bonding quadrupole modes, respectively.

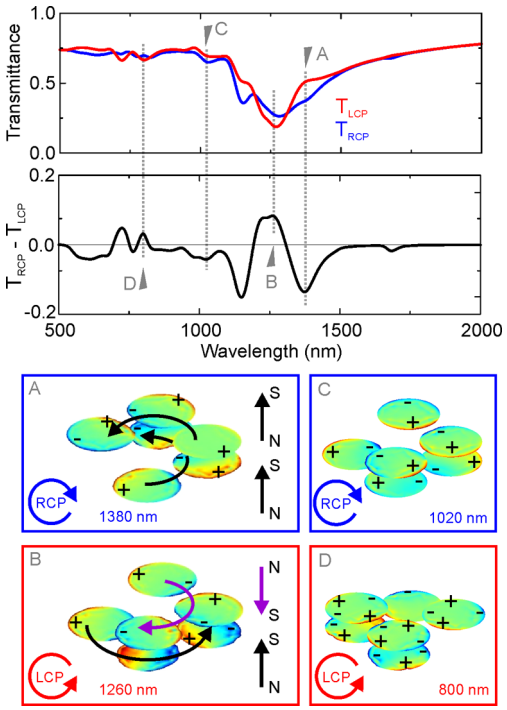

Figure 8. Calculated near- and far-field optical response of a two-layered chiral plasmonic oligomer, consisting of isolated particles. The two lowest energy modes at spectral positions A and B are the combination of the bonding dipole modes of the individual layers. Together with the displacement currents between the particles, we can define effective currents in each layer, giving rise to magnetic moments, similar to the case in Figure 7. The relative orientation of the magnetic moments determines the resonance energy of the modes. The higher energy modes at spectral positions C and D are as well basically combinations of higher order modes of the individual layers.

moments induced by these ring currents, which are sketched as purple and black arrows next to the corresponding field distribution. For the lowest energy mode, we see that the magnetic moments are aligned in parallel. This alignment is energetically favorable and reduces the resonance energy of the mode. In contrast, the magnetic moments for the higher energy mode at spectral position B are antiparallel, which raises the resonance energy.[5,70] The comparably large energy splitting between the two modes is thus due to the strong induced magnetic moments and their interaction. Importantly, when changing the handedness of the structure, the lowest energy mode will be the one under left-handed circularly polarized excitation, thus LCP and RCP switch their respective roles when changing the handedness of the structures. As it is not feasible to discuss all modes of the structure, we only show two additional representative cases. At spectral position C, we observe a bonding combination of two λ modes. At spectral position D, we observe a rather complicated mode profile which is the combination of two bonding quadrupole type modes. The shown near-field distributions thus underline that all observed modes are basically combinations of the fundamental modes of the individual building blocks, which are shown in Figure 6.

In Figure 8, we depict the calculations for the isolated particle structure. The calculated transmittance spectra for left- and right-handed circularly polarized excitation as well as the calculated ΔT spectrum are shown in the top part, the bottom part shows near-field distributions at four selected spectral positions. When examining the two energetically lowest modes A and B, one again finds a combination of the energetically lowest mode of the individual layer. The overall behavior is very similar to the previously discussed case of the merged L-shape. Despite the fact that there is no conductive coupling between the particles, we can again define ring currents in the individual layers. Even without a conductive bridge between the particles, the near-field coupling gives rise to displacement currents. The lowest energy mode is again characterized by parallel alignment of the induced magnetic moments, whereas the mode at slightly higher energy shows antiparallel alignment. In contrast to the merged L-shape, we only observe a weak splitting in resonance energy. The reason is the much smaller induced magnetic moment, as the ring

currents in the individual layers are significantly smaller due to the absence of conductive coupling. Additionally, we plot the field distributions for two higher order modes at spectral positions C and D. We again basically observe combinations of the fundamental modes of the individual layers. Yet, there is one pronounced difference which is important to note. As there is no conductive coupling between the individual particles of each layer, the particles are comparably weakly coupled as lateral plasmonic near-field coupling is weak. In contrast, the coupling between the particles stacked on top each other is significantly stronger. Therefore, the overall mode profiles are slightly distorted from the pure combinations of the modes of the individual layers as the coupling between the stacked particles of the two layers is more efficient.

CONCLUSIONS

In conclusion, we have studied in experiment and simulation the chiral optical response of stacked arrangements of metal nanoparticles, which we term three-dimensional chiral plasmonic oligomers. We have shown that the onset of charge transfer between the individual particles leads to an increased bandwidth extending from 700 to 3500 nm and an increased magnitude of the chiral optical response compared to the original oligomers. On the one hand, this is caused by the strong red shift of the fundamental mode at the onset of conductive coupling, shifting the chiral optical response to longer wavelength. On the other hand, due to the geometrical distortions of the particle, higher order modes of the structure can be excited with high efficiency and are hence responsible for the observed chiral optical response at higher energies. We have shown that the modes supported by the stacked structures are combinations of the modes of the individual layers. The lowest energy modes are associated with strong magnetic moments induced by ring currents inside the particles and displacement currents between them. The parallel or antiparallel alignment of these moments determines the energetic position of the respective modes and depends on the handedness of the structure and of the incident circularly polarized light.

We believe that the concept of three-dimensional chiral plasmonic oligomers together with the excitation of charge-transfer plasmon modes is a promising route for strong and broad-band chiral optical systems. These type of oligomers can be manufactured with a number of different strategies, such as DNA-guided self-assembly and subsequent metal overgrowth.[59]

Another intriguing possible application of three-dimensional plasmonic nanostructures is their use as 3D plasmon rulers.[71−73] Specific arrangements of metal nanoparticles are capable of encoding their 3D configuration optically, which would enable the inference of the full 3D arrangement of these particles from their optical response. In turn, one can as well deduce the configuration of a given optically inactive species attached to these chiral gold nanoparticle scaffolds. Chiral nanoparticle arrangements, such as our chiral plasmonic oligomers, are particularly suited for these type of applications, as chirality is a truly three-dimensional property.[43] The chiral optical response is very sensitive to small alterations of the configuration, which can even lead to a change of the handedness and therefore to a sign flip in the recorded CD spectrum. Three-dimensional plasmon rulers would offer an exciting opportunity for the observation of dynamic macromolecular dynamics. This would result in a highly important *in vivo* and *in situ* addition at the few-molecule level to other more conventional structural determination methods including macromolecular crystallography or NMR spectroscopy.

METHODS

Structure Fabrication. First, the quartz glass substrate (Suprasil, Heraeus) is covered with a 70 nm thick spacer layer by spin-coating. A solidifiable photopolymer, PC403 (JCR, Japan), is used. A prebaking process is first carried out to remove the solvent from the polymer (increase of the baking temperature from 90 to 130 °C). A sufficiently long bake at a higher temperature (30 min at 180 °C) further hardens the layer. Next the three-particle L-shape layer and alignment markers are defined in a resist (double-layer PMMA, Allresist) using electron-beam lithography (Raith e_Line). The substrate is then covered with a 2 nm Cr adhesion layer and a 40 nm gold film using thermal evaporation followed by a lift-off procedure. Subsequently, a 70 nm thick spacer layer of PC403 is applied. Afterward, the substrate is coated once more with a PMMA resist. Computer-controlled alignment using the gold alignment markers is applied to ensure the accurate positioning of the upper dot layer. Metal evaporation, lift off, and final planarization are repeated. All samples have a total area of 30 μm $\times$ 30 μm.

All scanning electron microscope (SEM) images are taken with a Hitachi S-4800 scanning electron microscope.

Optical Characterization. The spectra are measured using a Fourier transform infrared spectrometer (Bruker Vertex 80), equipped with an infrared microscope (Bruker Hyperion). The incident light is focused with a Cassegrain objective with numerical aperture = 0.4, and the transmitted intensities are detected with Si and InGaAs diodes as well as a liquid-nitrogen-cooled mercury cadmium telluride (MCT) detector. The incident polarization is set with infrared polarizers and two broad-band infrared quarter waveplates (700−2500 and 2500−7000 nm, B. Halle Nachfl., Berlin). The measured spectra are normalized with respect to the substrate.

Structure Dimensions. Each particle has a nominal gold thickness of 40 nm, with a 2 nm Cr adhesion layer. Due to the presence of a 70 nm thick dielectric spacer, the vertical distance between the particles is 30 nm. The center-to-center distance in the L-shape between the particles is 220 nm. The unit cell contains four oligomers each, rotated by 90° with respect to each other. The period within the unit cell is 650 nm in both directions. The unit cell period is 1500 nm in both directions. The difference between these periodicities has been chosen in order for the unit cell to be easily visible (cf. Figure 1c). The diameter *d* of the individual particles has been increased in six

steps in the experiment in order to observe the transition from capacitive to conductive coupling (cf. the structures in Figure 3). This results in 12 fields in total (two enantiomers each). The parameters have been extracted from SEM images and have been used in the simulations accordingly and are as follows: $d = 180, 200, 220, 240, 260, 280$ nm. Note that for $d = 220$ nm the particles of each layer have just started to touch.

Simulations. In the simulation, three-dimensional Maxwell's equations are solved using the finite element method (COMSOL Multiphysics finite element analysis simulation software). The dielectric function of gold is taken from the Palik handbook.[74] A unit cell consisting of four elements arranged in the C_4-symmetric fashion was simulated, which is the same as the fabricated structure shown in Figure 1c. At the sides of the unit cell, periodic boundary condition is assumed in order to obtain the optical response of the whole oligomer array. A normal incident circularly polarized light source (500−3500 nm) is used. As the incident light wave strikes the structure, it will be absorbed, reflected, or transmitted through the structure. The absorbed power is computed through the volume integration of the resistive heating in the gold nanoparticles. The reflected or transmitted power is calculated through the surface integration of the power flow over the surfaces far away from the nanoparticle layers. The sum of calculated power of absorption, reflection, and transmission is checked against the incident power to ensure the accuracy of simulation. In addition, the near-field information at the resonant wavelengths in which we are interested can be directly obtained from the simulations, as well. The mode images in Figures 5−8 show the distributions of electric fields perpendicular to the layers, and they are taken at the top layer of the nanodiscs.

Conflict of Interest: The authors declare no competing financial interest.

Acknowledgment. M.H., M.S., and H.G. gratefully acknowledge financial support by Deutsche Forschungsgemeinschaft (SPP1391, FOR730, and GI 269/11-1), by BMBF (13N9048 and 13N10146), by Baden-Württemberg Stiftung, and by German−Israeli Foundation. L.W., P.B., and E.P.L. acknowledge the financial support by Agency for Science and Technology Research (A*STAR) Singapore with Thematic Strategic Research Programme (TSRP) Grants: iNPBi−LSPR POC for Clinical Screening and Medical Diagnostics No. 102152 0014, and Metamaterials−Nanoplasmonics No. 0921540098. The authors would like to thank Sven Hein for his visualizations.

REFERENCES AND NOTES

1. Barron, L. D. *Molecular Light Scattering and Optical Activity*, 2nd ed.; Cambridge University Press: Cambridge, UK, 2004.
2. Gansel, J. K.; Thiel, M.; Rill, M. S.; Decker, M.; Bade, K.; Saile, V.; Freymann, G.; von Linden, S.; Wegener, M. Gold Helix Photonic Metamaterial as Broadband Circular Polarizer. *Science* **2009**, *325*, 1513–1515.
3. Gansel, J. K.; Latzel, M.; Frölich, A.; Kaschke, J.; Thiel, M.; Wegener, M. Tapered Gold-Helix Metamaterials as Improved Circular Polarizers. *Appl. Phys. Lett.* **2012**, *100*, 101109.
4. Radke, A.; Gissibl, T.; Klotzbücher, T.; Braun, P. V.; Giessen, H. Three-Dimensional Bichiral Plasmonic Crystals Fabricated by Direct Laser Writing and Electroless Silver Plating. *Adv. Mater.* **2011**, *23*, 3018–3021.
5. Liu, N.; Liu, H.; Zhu, S.; Giessen, H. Stereometamaterials. *Nat. Photonics* **2009**, *3*, 157–162.
6. Decker, M.; Ruther, M.; Kriegler, C. E.; Zhou, J.; Soukoulis, C. M.; Linden, S.; Wegener, M. Strong Optical Activity from Twisted-Cross Photonic Metamaterials. *Opt. Lett.* **2009**, *34*, 2501–2503.
7. Helgert, C.; Pshenay-Severin, E.; Falkner, M.; Menzel, C.; Rockstuhl, C.; Kley, E.-B.; Tünnermann, A.; Lederer, F.; Pertsch, T. Chiral Metamaterial Composed of Three-Dimensional Plasmonic Nanostructures. *Nano Lett.* **2011**, *11*, 4400–4404.
8. Menzel, C.; Helgert, C.; Rockstuhl, C.; Kley, E.-B.; Tünnermann, A.; Pertsch, T.; Lederer, F. Asymmetric Transmission of Linearly Polarized Light at Optical Metamaterials. *Phys. Rev. Lett.* **2010**, *104*, 253902.
9. Zhu, Z.; Liu, W.; Li, Z.; Han, B.; Zhou, Y.; Gao, Y.; Tang, Z. Manipulation of Collective Optical Activity in One Dimensional Plasmonic Assembly. *ACS Nano* **2012**, *6*, 2326–2332.
10. Guerrero-Martínez, A.; Alonso-Gómez, J. L.; Auguié, B.; Cid, M. M.; Liz-Marzán, L. M. From Individual to Collective Chirality in Metal Nanoparticles. *Nano Today* **2011**, *6*, 381–400.
11. Shemer, G.; Krichevski, O.; Markovich, G.; Molotsky, T.; Lubitz, I.; Kotlyar, A. B. Chirality of Silver Nanoparticles Synthesized on DNA. *J. Am. Chem. Soc.* **2006**, *128*, 11006–11007.
12. Zhao, Y.; Belkin, M. A.; Alù, A. Twisted Optical Metamaterials for Planarized Ultrathin Broadband Circular Polarizers. *Nat. Commun.* **2012**, *3*, 870.
13. Christofi, A.; Stefanou, N.; Gantzounis, G.; Papanikolaou, N. Giant Optical Activity of Helical Architectures of Plasmonic Nanorods. *J. Phys. Chem. C* **2012**, *116*, 16674–16679.
14. Fan, Z.; Govorov, A. O. Chiral Nanocrystals: Plasmonic Spectra and Circular Dichroism. *Nano Lett.* **2012**, *12*, 3283–3289.
15. Menzel, C.; Rockstuhl, C.; Paul, T.; Lederer, F. Retrieving Effective Parameters for Quasiplanar Chiral Metamaterials. *Appl. Phys. Lett.* **2008**, *93*, 233106.
16. Papakostas, A.; Potts, A.; Bagnall, D.; Prosvirnin, S.; Coles, H.; Zheludev, N. Optical Manifestations of Planar Chirality. *Phys. Rev. Lett.* **2003**, *90*, 107404.
17. Plum, E.; Liu, X.-X.; Fedotov, V.; Chen, Y.; Tsai, D.; Zheludev, N. Metamaterials: Optical Activity without Chirality. *Phys. Rev. Lett.* **2009**, *102*, 113902.
18. Canfield, B. K.; Kujala, S.; Kauranen, M.; Jefimovs, K.; Vallius, T.; Turunen, J. Remarkable Polarization Sensitivity of Gold Nanoparticle Arrays. *Appl. Phys. Lett.* **2005**, *86*, 183109.
19. Kuwata-Gonokami, M.; Saito, N.; Ino, Y.; Kauranen, M.; Jefimovs, K.; Vallius, T.; Turunen, J.; Svirko, Y. Giant Optical Activity in Quasi-Two-Dimensional Planar Nanostructures. *Phys. Rev. Lett.* **2005**, *95*, 227401.
20. Canfield, B. K.; Kujala, S.; Laiho, K.; Turunen, J.; Kauranen, M. Chirality Arising from Small Defects in Gold Nanoparticle Arrays. *Opt. Express* **2006**, *14*, 563–565.
21. Eftekhari, F.; Davis, T. Strong Chiral Optical Response from Planar Arrays of Subwavelength Metallic Structures Supporting Surface Plasmon Resonances. *Phys. Rev. B* **2012**, *86*, 075428.
22. Decker, M.; Klein, M. W.; Wegener, M.; Linden, S. Circular Dichroism of Planar Chiral Magnetic Metamaterials. *Opt. Lett.* **2007**, *32*, 856–858.
23. Halas, N. J.; Lal, S.; Chang, W.-S.; Link, S.; Nordlander, P. Plasmons in Strongly Coupled Metallic Nanostructures. *Chem. Rev.* **2011**, *111*, 3913–3961.
24. Artar, A.; Yanik, A. A.; Altug, H. Multispectral Plasmon Induced Transparency in Coupled Meta-Atoms. *Nano Lett.* **2011**, *11*, 1685–1689.
25. Gallinet, B.; Martin, O. J. F. Influence of Electromagnetic Interactions on the Line Shape of Plasmonic Fano Resonances. *ACS Nano* **2011**, *5*, 8999–9008.
26. Barrow, S. J.; Funston, A. M.; Gómez, D. E.; Davis, T. J.; Mulvaney, P. Surface Plasmon Resonances in Strongly Coupled Gold Nanosphere Chains from Monomer to Hexamer. *Nano Lett.* **2011**, *11*, 4180–4187.
27. Slaughter, L. S.; Willingham, B. A.; Chang, W.-S.; Chester, M. H.; Ogden, N.; Link, S. Toward Plasmonic Polymers. *Nano Lett.* **2012**, *12*, 3967–3972.
28. Frimmer, M.; Coenen, T.; Koenderink, A. F. Signature of a Fano Resonance in a Plasmonic Metamolecule's Local Density of Optical States. *Phys. Rev. Lett.* **2012**, *108*, 077404.
29. Artar, A.; Yanik, A. A.; Altug, H. Directional Double Fano Resonances in Plasmonic Hetero-oligomers. *Nano Lett.* **2011**, *11*, 3694–3700.
30. Rahmani, M.; Lei, D. Y.; Giannini, V.; Lukiyanchuk, B.; Ranjbar, M.; Liew, T. Y. F.; Hong, M.; Maier, S. A. Subgroup Decomposition of Plasmonic Resonances in Hybrid Oligomers: Modeling the Resonance Lineshape. *Nano Lett.* **2012**, *12*, 2101–2106.
31. Wu, C.; Khanikaev, A. B.; Adato, R.; Arju, N.; Yanik, A. A.; Altug, H.; Shvets, G. Fano-Resonant Asymmetric Metamaterials for Ultrasensitive Spectroscopy and Identification of Molecular Monolayers. *Nat. Mater.* **2011**, *11*, 69–75.

32. Ament, I.; Prasad, J.; Henkel, A.; Schmachtel, S.; Sönnichsen, C. Single Unlabeled Protein Detection on Individual Plasmonic Nanoparticles. *Nano Lett.* **2012**, *12*, 1092–1095.
33. Zijlstra, P.; Paulo, P. M. R.; Orrit, M. Optical Detection of Single Non-absorbing Molecules Using the Surface Plasmon Resonance of a Gold Nanorod. *Nat. Nanotechnol.* **2012**, *7*, 379–382.
34. Rodríguez-Lorenzo, L.; de la Rica, R.; Alvarez-Puebla, R. A.; Liz-Marzán, L. M.; Stevens, M. M. Plasmonic Nanosensors with Inverse Sensitivity by Means of Enzyme-Guided Crystal Growth. *Nat. Mater.* **2012**, *11*, 604–607.
35. Tang, Y.; Cohen, A. E. Enhanced Enantioselectivity in Excitation of Chiral Molecules by Superchiral Light. *Science* **2011**, *332*, 333–336.
36. Bliokh, K.; Nori, F. Characterizing Optical Chirality. *Phys. Rev. A* **2011**, *83*, 021803(R).
37. Tang, Y.; Cohen, A. E. Optical Chirality and Its Interaction with Matter. *Phys. Rev. Lett.* **2010**, *104*, 163901.
38. Schäferling, M.; Dregely, D.; Hentschel, M.; Giessen, H. Tailoring Enhanced Optical Chirality: Design Principles for Chiral Plasmonic Nanostructures. *Phys. Rev. X* **2012**, *2*, 031010.
39. Hendry, E.; Carpy, T.; Johnston, J.; Popland, M.; Mikhaylovskiy, R. V.; Lapthorn, A. J.; Kelly, S. M.; Barron, L. D.; Gadegaard, N.; Kadodwala, M. Ultrasensitive Detection and Characterization of Biomolecules Using Superchiral Fields. *Nat. Nanotechnol.* **2010**, *5*, 783–787.
40. Govorov, A. O.; Fan, Z.; Hernandez, P.; Slocik, J. M.; Naik, R. R. Theory of Circular Dichroism of Nanomaterials Comprising Chiral Molecules and Nanocrystals: Plasmon Enhancement, Dipole Interactions, and Dielectric Effects. *Nano Lett.* **2010**, *10*, 1374–1382.
41. Govorov, A. O. Plasmon-Induced Circular Dichroism of a Chiral Molecule in the Vicinity of Metal Nanocrystals. Application to Various Geometries. *J. Phys. Chem. C* **2011**, *115*, 7914–7923.
42. Abdulrahman, N. A.; Fan, Z.; Tonooka, T.; Kelly, S. M.; Gadegaard, N.; Hendry, E.; Govorov, A. O.; Kadodwala, M. Induced Chirality through Electromagnetic Coupling between Chiral Molecular Layers and Plasmonic Nanostructures. *Nano Lett.* **2012**, *12*, 977–983.
43. Hentschel, M.; Schäferling, M.; Weiss, T.; Liu, N.; Giessen, H. Three-Dimensional Chiral Plasmonic Oligomers. *Nano Lett.* **2012**, *12*, 2542–2547.
44. Atay, T.; Song, J.-H.; Nurmikko, A. V. Strongly Interacting Plasmon Nanoparticle Pairs: From Dipole−Dipole Interaction to Conductively Coupled Regime. *Nano Lett.* **2004**, *4*, 1627–1631.
45. Lassiter, J. B.; Aizpurua, J.; Hernandez, L. I.; Brandl, D. W.; Romero, I.; Lal, S.; Hafner, J. H.; Nordlander, P.; Halas, N. J. Close Encounters between Two Nanoshells. *Nano Lett.* **2008**, *8*, 1212–1218.
46. Romero, I.; Aizpurua, J.; Bryant, G. W.; García De Abajo, F. J. Plasmons in Nearly Touching Metallic Nanoparticles: Singular Response in the Limit of Touching Dimers. *Opt. Express* **2006**, *14*, 9988–9999.
47. Pérez-González, O.; Zabala, N.; Borisov, A. G.; Halas, N. J.; Nordlander, P.; Aizpurua, J. Optical Spectroscopy of Conductive Junctions in Plasmonic Cavities. *Nano Lett.* **2010**, *10*, 3090–3095.
48. Esteban, R.; Borisov, A. G.; Nordlander, P.; Aizpurua, J. Bridging Quantum and Classical Plasmonics with a Quantum-Corrected Model. *Nat. Commun.* **2012**, *3*, 825.
49. Neubrech, F.; Garcia-Etxarri, A.; Weber, D.; Bochterle, J.; Shen, H.; Lamy de la Chapelle, M.; Bryant, G. W.; Aizpurua, J.; Pucci, A. Defect-Induced Activation of Symmetry Forbidden Infrared Resonances in Individual Metallic Nanorods. *Appl. Phys. Lett.* **2010**, *96*, 213111.
50. Alber, I.; Sigle, W.; Demming-Janssen, F.; Neumann, R.; Trautmann, C.; van Aken, P. A.; Toimil-Molares, M. E. Multipole Surface Plasmon Resonances in Conductively Coupled Metal Nanowire Dimers. *ACS Nano* **2012**, 10.1021/nn303149p.
51. Thiel, M.; Rill, M. S.; Freymann, G.; von Wegener, M. Three-Dimensional Bi-chiral Photonic Crystals. *Adv. Mater.* **2009**, *21*, 4680–4682.
52. Stefik, M.; Wang, S.; Hovden, R.; Sai, H.; Tate, M. W.; Muller, D. A.; Steiner, U.; Gruner, S. M.; Wiesner, U. Networked and Chiral Nanocomposites from ABC Triblock Terpolymer Coassembly with Transition Metal Oxide Nanoparticles. *J. Mater. Chem.* **2012**, *22*, 1078–1087.
53. Vignolini, S.; Yufa, N. A.; Cunha, P. S.; Guldin, S.; Rushkin, I.; Stefik, M.; Hur, K.; Wiesner, U.; Baumberg, J. J.; Steiner, U. A 3D Optical Metamaterial Made by Self-Assembly. *Adv. Mater.* **2012**, *24*, OP23–OP27.
54. Dupont, J.; Liu, G.; Niihara, K.; Kimoto, R.; Jinnai, H. Self-Assembled ABC Triblock Copolymer Double and Triple Helices. *Angew. Chem., Int. Ed.* **2009**, *48*, 6144–6147.
55. Ho, R.-M.; Chen, C.-K.; Chiang, Y.-W. Novel Nanostructures from Self-Assembly of Chiral Block Copolymers. *Macromol. Rapid Commun.* **2009**, *30*, 1439–1456.
56. Chen, W.; Bian, A.; Agarwal, A.; Liu, L.; Shen, H.; Wang, L.; Xu, C.; Kotov, N. A. Nanoparticle Superstructures Made by Polymerase Chain Reaction: Collective Interactions of Nanoparticles and a New Principle for Chiral Materials. *Nano Lett.* **2009**, *9*, 2153–2159.
57. Mastroianni, A. J.; Claridge, S. A.; Alivisatos, A. P. Pyramidal and Chiral Groupings of Gold Nanocrystals Assembled Using DNA Scaffolds. *J. Am. Chem. Soc.* **2009**, *131*, 8455–8459.
58. Chen, C.-L.; Zhang, P.; Rosi, N. L. A New Peptide-Based Method for the Design and Synthesis of Nanoparticle Superstructures: Construction of Highly Ordered Gold Nanoparticle Double Helices. *J. Am. Chem. Soc.* **2008**, *130*, 13555–13557.
59. Kuzyk, A.; Schreiber, R.; Fan, Z.; Pardatscher, G.; Roller, E.-M.; Högele, A.; Simmel, F. C.; Govorov, A. O.; Liedl, T. DNA-Based Self-Assembly of Chiral Plasmonic Nanostructures with Tailored Optical Response. *Nature* **2012**, *483*, 311–314.
60. Shen, X.; Song, C.; Wang, J.; Shi, D.; Wang, Z.; Liu, N.; Ding, B. Rolling up Gold Nanoparticle-Dressed DNA Origami into Three-Dimensional Plasmonic Chiral Nanostructures. *J. Am. Chem. Soc.* **2012**, *134*, 146–149.
61. Decker, M.; Zhao, R.; Soukoulis, C. M.; Linden, S.; Wegener, M. Twisted Split-Ring-Resonator Photonic Metamaterial with Huge Optical Activity. *Opt. Lett.* **2010**, *35*, 1593–1595.
62. Castro-Lopez, M.; Brinks, D.; Sapienza, R.; van Hulst, N. F. Aluminum for Nonlinear Plasmonics: Resonance-Driven Polarized Luminescence of Al, Ag, and Au Nanoantennas. *Nano Lett.* **2011**, *11*, 4674–4678.
63. Jakab, A.; Rosman, C.; Khalavka, Y.; Becker, J.; Trügler, A.; Hohenester, U.; Sönnichsen, C. Highly Sensitive Plasmonic Silver Nanorods. *ACS Nano* **2011**, *5*, 6880–6885.
64. Fredriksson, H.; Alaverdyan, Y.; Dmitriev, A.; Langhammer, C.; Sutherland, D. S.; Zäch, M.; Kasemo, B. Hole−Mask Colloidal Lithography. *Adv. Mater.* **2007**, *19*, 4297–4302.
65. Liu, N.; Guo, H.; Fu, L.; Kaiser, S.; Schweizer, H.; Giessen, H. Three-Dimensional Photonic Metamaterials at Optical Frequencies. *Nat. Mater.* **2008**, *7*, 31–37.
66. Slaughter, L. S.; Wu, Y.; Willingham, B. A.; Nordlander, P.; Link, S. Effects of Symmetry Breaking and Conductive Contact on the Plasmon Coupling in Gold Nanorod Dimers. *ACS Nano* **2010**, *4*, 4657–4666.
67. Berova, N.; Nakanishi, K.; Woody, R. W. Circular Dichroism. *Principles and Applications*; Wiley: New York, 2000.
68. Wu, L.; Bai, P.; Li, E. P. Designing Surface Plasmon Resonance of Subwavelength Hole Arrays by Studying Absorption. *J. Opt. Soc. Am. B* **2012**, *29*, 521–528.
69. Husu, H.; Mäkitalo, J.; Laukkanen, J.; Kuittinen, M.; Kauranen, M. Particle Plasmon Resonances in L-Shaped Gold Nanoparticles. *Opt. Express* **2010**, *18*, 16601–16606.
70. Liu, N.; Giessen, H. Coupling Effects in Optical Metamaterials. *Angew. Chem., Int. Ed.* **2010**, *49*, 9838–9852.
71. Sönnichsen, C.; Reinhard, B. M.; Liphardt, J.; Alivisatos, A. P. A Molecular Ruler Based on Plasmon Coupling of Single Gold and Silver Nanoparticles. *Nat. Biotechnol.* **2005**, *23*, 741–745.

72. Liu, N.; Hentschel, M.; Weiss, T.; Alivisatos, A. P.; Giessen, H. Three-Dimensional Plasmon Rulers. *Science* **2011**, *332*, 1407–1410.
73. Davis, T. J.; Hentschel, M.; Liu, N.; Giessen, H. Analytical Model of the Three-Dimensional Plasmonic Ruler. *ACS Nano* **2012**, *6*, 1291–1298.
74. Palik, E. D. *Handbook of Optical Constants of Solids*; Academic: New York, 1998.